ELSEVIER

Materials Science and Engineering B69–70 (2000) 386–391

MATERIALS SCIENCE & ENGINEERING B

www.elsevier.com/locate/mseb

Structural evolution of SnO_2–TiO_2 nanocrystalline films for gas sensors

Felix Edelman [a,*], Horst Hahn [a], Stefan Seifried [a], Christian Alof [a], Holger Hoche [a], Adam Balogh [a], Peter Werner [b], Katarzyna Zakrzewska [c], Marta Radecka [c], Pawel Pasierb [c], Albert Chack [c], Vissarion Mikhelashvili [d], Ghadi Eisenstein [d]

[a] *Materials Engineering Faculty, Technical University of Darmstadt, 64287 Darmstadt, Germany*
[b] *Max Planck Institute of Microstructure Physics, Halle/Saale D-06120, Germany*
[c] *University of Mining and Metallurgy, 30-059 Cracow, Poland*
[d] *Technion-Israel Institute of Technology, 32000 Haifa, Israel*

Abstract

Thin films (50–200 nm) of SnO_2–TiO_2 were deposited on SiO_2/(001)Si substrates by RF-sputtering and by molecular beam before they were annealed in vacuum at 200–900°C. In-situ TEM, XRD, SEM, Raman and IR-spectroscopy were used to analyze the structure transformations in the SnO_2–TiO_2 films. In the as-deposited state, the films are amorphous. They crystallize at higher temperatures (starting at about 500°C) forming nanosized grains. The problem of the spinodal decomposition in the SnO_2–TiO_2 system observed earlier at high temperatures is discussed also for low-temperature processing. The stoichiometry of the films of both groups (reactive ion sputtered and high-vacuum e-gun sputtered) is being compared. © 2000 Elsevier Science S.A. All rights reserved.

Keywords: Titanium oxide; Tin oxide; Gas sensors; Nanocrystalline films

1. Introduction

Metal–oxide semiconductor thin films are promising for gas sensors due to the dependence of their electrical conductivity on the environmental gases such as, e.g. O_2, CO, H_2O, NO_x, etc. [1–3]. Two main mechanisms are responsible for gas sensing. (A) The bulk diffusion of oxygen from outside into the oxide, compensating an original deficiency of oxygen, which is typical of most metal oxides (occupation of O-vacancies as the donor centers, in the oxide increases the resistivity). These oxygen-sensitive devices are working at high temperatures mainly in combustion systems. A material for the latter is a Ti-oxide in the crystalline form (rutile, anatase) or a ZrO_2-oxide. (B) The low-temperature chemisorption (at 100–500°C) of environmental gases on the surface of multiple grains, changing the surface state and charge distribution inside the grains and therefore governing the resistivity of polycrystalline films. A material typical of B-type sensors is a Sn-oxide, preferentially in the cassiterite form. Area of B-sensors use is reducing gas (H_2, CO, etc.) detection. Metal-oxide sensors produced via sintering, sol-gel processes (in the case of thick films) or by reactive ion sputtering (RIS) and e-gun sputtering (EGS) build up the films, which are thin and porous. The pores serve as channels for the gas transport to provide the material resistivity response and, on the other hand, the gas evacuates through the pores during recovery. The pore fraction within the metal-oxide structure reaches at least 10–20%. TiO_2-sensors are sufficiently sensitive only at elevated temperatures and stable up to 800–1000°C. The relatively low-conductive mixture of amorphous/rutile TiO_2 films deposited by RIS showed better sensing properties than that of EGS–TiO_2 amorphous/anatase films [4]. Above 400–500°C (oxygen losses), the low-temperature SnO_2-sensors suffer from a structure instability and poor selectivity. The SnO_2–TiO_2 system seems to combine the positive features of both sensor materials, viz. SnO_2 and TiO_2.

The equilibrium phase diagram of the SnO_2–TiO_2 system, obtained only above 800–900°C, presents a solid solution with a miscibility gap [5]. Detailed studies

* Corresponding author.
E-mail address: felixe@hrzpub.tu-darmstadt.de (F. Edelman)

0921-5107/00/$ - see front matter
PII: S0921-5107(99)00282-2

of the solid solution spinodal decomposition [6–10,16] showed that the non-decomposed part of the solid solution diagram occupies only narrow areas of about 0–15% close to the SnO_2 or TiO_2 corners, respectively. The spinodal decomposition process is represented morphologically in the formation of lamellar multilayers (in monocrystalline bulk SnO_2–TiO_2).

Recently, SnO_2–TiO_2 ceramics and films with about 5–10% TiO_2 (out of the high-temperature miscibility gap) were suggested to be applied as high-temperature resistors [11] and to sensors for hydrocarbons and hydrogen gases [12–14], always to increase the upper temperature limit of the device stability.

The paper presents a comparative analysis of SnO_2–TiO_2 films deposited by both RIS and molecular beam (MB, version of the EGS) techniques, emphasizing decomposition features in the solid solution, that govern the temperature stability of the structure of the sensor.

2. Experimental

We used two types of SnO_2–TiO_2 films: (a) rf reactive ion sputtered (RIS) from Ti–Sn metallic mosaic targets (see [14]), and (b) deposited by means of electron gun molecular beam (MB) sputtering from SnO_2 and TiO_2 targets. During deposition the substrates were kept at a temperature of 200°C. The films were deposited on SiO_2/(001)Si, glass and on cleaved NaCl crystals (for TEM). The film thickness ranged from 50–200 nm. Rutherford backscattering and electron probe microanalysis (EPMA) were used for compositional analysis. Both the RIS and MB SnO_2–TiO_2 films, usually amorphous in the as-deposited state, were annealed in a hot-wall furnace at a vacuum of $\sim 10^{-5}$ Pa at temperatures between 200 and 850°C or in situ in a JEM-1000 microscope (1 MeV acceleration voltage) in the same temperature range. The film morphology was studies by high-resolution SEM. For the XRD analysis, we used the grazing beam geometry. The optical properties were determined by optical spectroscopy.

With respect to their composition, the plasma-deposited RIS-films were more stoichiometric than the MB ones deposited in high vacuum. The latter ones were characterized by some deficiency of oxygen (5–20%), especially the SnO_2-rich films.

3. Results and discussion

3.1. Film morphology

A smooth relief of RIS and MB-films is typical after the films deposition and after their annealing in vacuum up to 500°C. It is interesting that further annealing SnO_2-rich SnO_2–TiO_2 MB films at higher temperatures (Fig. 1a, 700°C, 1 h) leads in the case of the SnO_x phase separation (white snowflakes-like hillocks, the composition of which is analyzed by EPMA). With annealing temperature increasing the hillocks vanish and the film relief sharpens (Fig. 1b, 800°C, 1 h). After annealing $SnO_2/TiO_2 = 50/50$ for 1 h at 500°C the MB films show morphology of large grains.

3.2. XRD analysis of thick ($\sim$ 200 nm) films deposited on SiO_2/Si substrates

The phase analysis of the RIS SnO_2–TiO_2 films performed earlier [14,15,17] show that in the as-deposited state and after annealing, the SnO_2 films display a cassiterite phase, the TiO_2 films are rutile/anatase mixtures and the intermediate compositions are predominantly mixtures of solid solutions based on SnO_2 and TiO_2 compounds as it was shown for bulk ceramic samples annealed at $T \gg 800$°C [5–10]. In this study, the structure of the pure SnO_2 and TiO_2 samples was comparable to that of cassiterite and rutile/anatase, respectively. The XRD features of titania films were typical of anatase similarly to the e-gun films deposited in high vacuum [4]. The tin-oxide MB-films in the as-deposited state were partially reduced showing XRD spectra typical of SnO_x phases (mixtures of cassiterite SnO_2, Sn_3O_4 and SnO). In the SnO_2–TiO_2 film contained 30% SnO_2, the structure of the non-decomposed

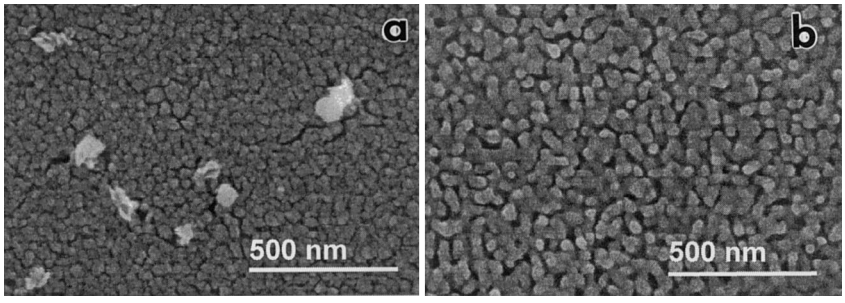

Fig. 1. SEM of molecular-beam deposited SnO_2–TiO_2 films (70%SnO_2) after vacuum annealing for 1 h at 700 (a) and 800°C (b).

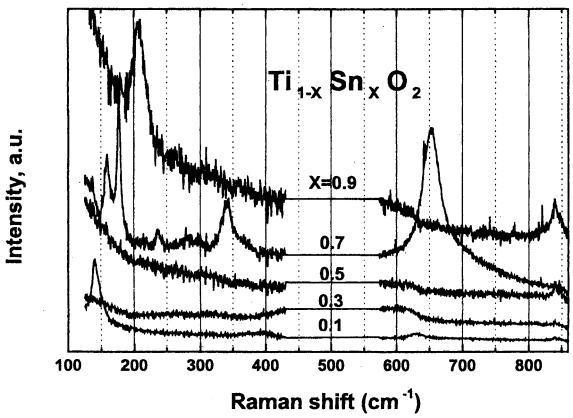

Fig. 2. Raman spectra of TiO_2–SnO_2 ($Ti_{1-x}Sn_xO_2$) MB-films with $x = 0.1$ to 0.9.

solid solution remained unchanged (with the corresponding XRD peak position fixed) from the as-deposited state up to 850°C. Only the crystalline phase and the crystals were increasing in size with rising annealing temperature. For the SnO_2–TiO_2 50/50 alloy, after annealing at 700–850°C we obtained the non-decomposed solid solution with a lattice spacing between cassiterite and rutile. However, in the tin-oxide rich films (70% SnO_2) the typical structure was a mixture of rutile, cassiterite, tin and titanium suboxides (Magneli phases [18], Ti_9O_{17} and $Ti_{10}O_{19}$).

3.3. Raman spectroscopy

The Raman spectra of nanocrystalline tin-dioxide [19,20] and titanium-dioxide [21,22] as two tetragonal compounds of the rutile type are well-known and have been characterized in detail. Recently, the Raman spectroscopy technique was applied to the SnO_2–TiO_2 system to reveal the spinodal decomposition features in the ceramic (bulk) state [23] and in the form of the sol–gel films [24]. Coherent (001) spinodals manifesting the decomposition effect were detected in ceramic samples, but no decomposition was observed in $Ti_{1-x}Sn_xO_2$ film samples with $x = 0.3$ to 0.6, the lattice of which, nevertheless, showed strong octahedral distortion.

Fig. 2 shows Raman spectra of our 'thick' $Ti_{1-x}Sn_xO_2$ MB-films with $x = 0.1$ to 0.9 after annealing at 500°C for 1 h (spectra area range between ~ 420 and 570 cm^{-1} were excluded due to a strong parasitic Si-substrate signal at ~ 520 cm^{-1}). The regular shift of the E_g-peaks from the TiO_2 position to the SnO_2 one, is probably typical of suboxidic mixtures, is remarkable. We believe that the small peak at 840 cm^{-1}, the intensity of which slightly increases with x as a specific characteristic to the SnO_2-component, proves that some SnO_2 clusters are stable throughout the film. A strong peak A_{1g} (~ 650 cm^{-1}) at $x = 0.7$ surely belongs to the separated SnO_2 phase. Therefore, Raman spectra can be considered to favor the model of mixed solid solutions (decomposition).

3.4. Optical absorption spectroscopy

The optical gap obtained by using the FT-spectra of the 'thick' MB-films (on glass) can be separated into three groups for $Ti_{1-x}Sn_xO_2$ with $x = 0$ to 1 (we use this simple complex formula notwithstanding of some of oxygen film nonstoichiometry 'y', more accurate would be $Ti_{1-x}Sn_xO_{2-y}$):

1. $x = 1$–0.7, W(opt.) = 2.22.4 eV for the films crystallized at 500°C, and for the as-deposited films that are amorphous or semi-crystalline, respectively;
2. $x = 0$–0.3, W(opt.) = 3.2–3.37 eV for the films crystallized at 500°C, and for the as-deposited films that are amorphous or semi-crystalline at 500°C, respectively;
3. $x = 0.4$–0.6 representing the very interesting case of the 'two-gap state' with a two-shoulder optical absorption slope, one-typical of SnO_2, another one-typical of TiO_2. Fig. 3 shows the film of $SnO_2/TiO_2 = 50/50$, in the as-deposited state (curve 1: the slopes correspond to 2.4 and 3.1 eV for SnO_2 and TiO_2 component, respectively) and after annealing at $T = 500$°C (curve 2: the slopes correspond to 2.4 and 2.95 eV, for SnO_2 and TiO_2 component, respectively).

Compared with the data of Raman spectroscopy, the optical absorption data show a better agreement with the two-phase mixture mode of the TiO_2–SnO_2 system not only in the crystallized state but also in the as-deposited amorphous or semi-crystalline state.

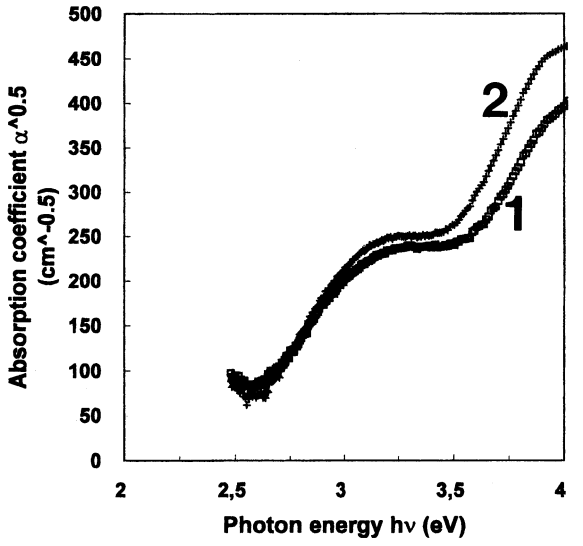

Fig. 3. IR-spectra of the MB-film of 50%SnO_2/50%TiO_2 in the as-deposited state (amorphous, curve 1) and annealed at 500°C for 15 min in vacuum (amorphous + anatase + Sn-suboxides, curve 2).

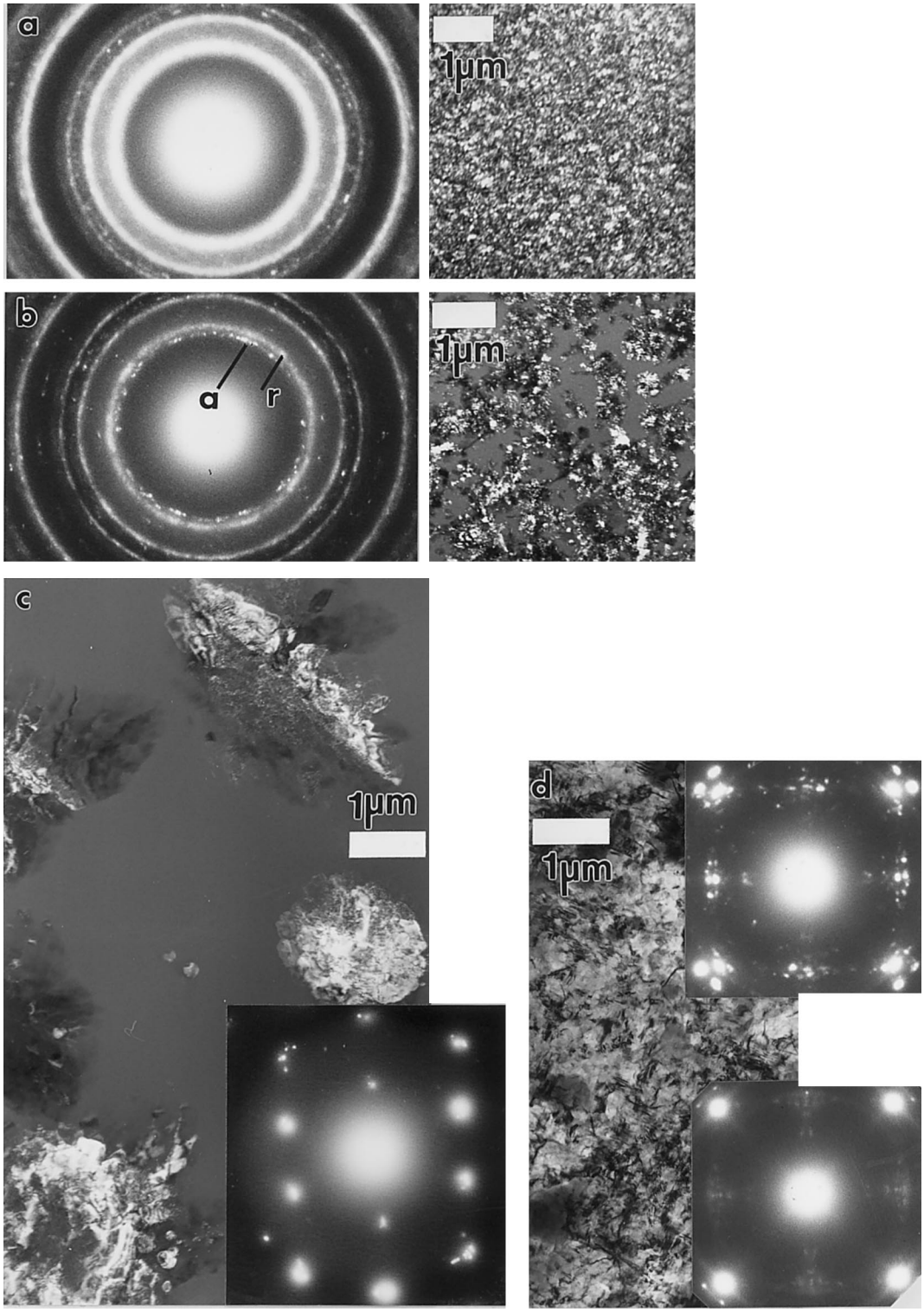

Fig. 4. Plane-view TEM micrographs of SnO_2 and TiO_2 films during in situ annealing: (a) RIS–SnO_2, 600°C, 15 min, cassiterite; (b) RIS–TiO_2, 500°C, 1 h, rutile (*r*) and anatase (a) mixture (the '*r*' and '*a*' reflections are shown in corresponding selected area diffraction (SAD) images); (c) MB–TiO_2, 550°C, 15 min, anatase, and (d) MB–SnO_2 film crystallized on NaCl substrate in the as-deposited state showing a layered structure of cassiterite and Sn-suboxides. Figures (a), (b) and (c) are dark-field images, (d) is bright-field one.

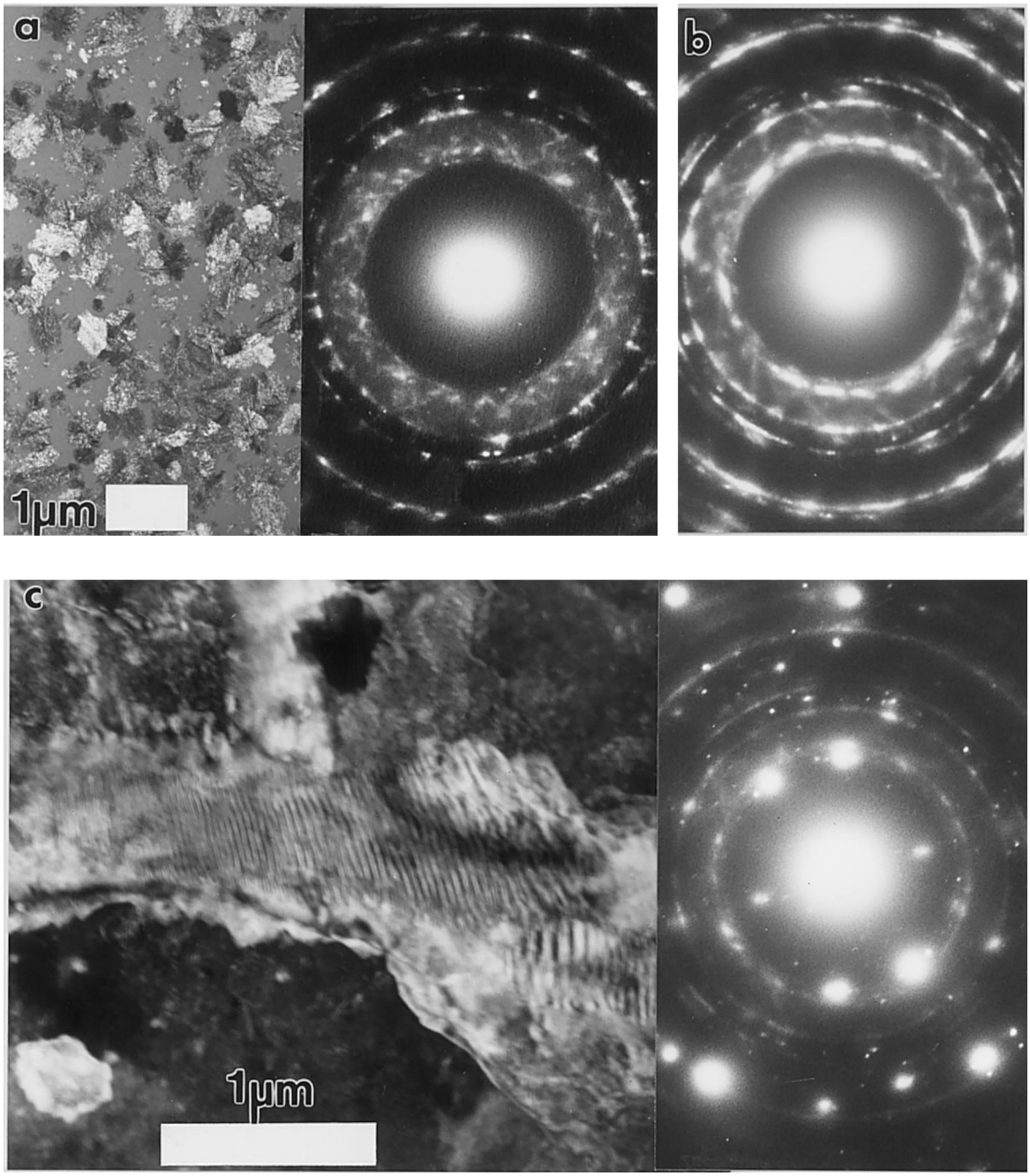

Fig. 5. Plane-view TEM micrographs (dark-field) of SnO_2–TiO_2 RIS films during in situ annealing: (a) 10%SnO_2/90%TiO_2, 550°C, 15 min; (b) diffraction features in as in Fig. 5a but here for the film with 35% SnO_2; (c) layered decomposition of the 10%SnO_2/90%TiO_2 MB-film into the Sn-suboxides and anatase TiO_2 crystals.

3.5. TEM in situ analysis of thin (∼50 nm) films deposited on rock salt

Fig. 4 and Fig. 5 show the RIS and MB SnO_2–TiO_2 after their in situ crystallization. The main results of the TEM investigations are:

1. In the as-deposited state RIS SnO_2 films are amorphous and crystallize at temperatures above 700°C forming mainly cassiterite crystals with probably a small amount of Sn-suboxides (that manifests in diffraction rings broadering in the area of ∼2.5 to 3.5 Å, which is typical of strong suboxide reflections). Crystallization occurs via an extraordinary high nucleation rate but the crystal growth rate is low. The resulting structure is nanocrystalline with an average grain size of 10–50 nm (Fig. 4a).
2. RIS TiO_2 films start to crystallize at ∼500°C, occuring as mixtures of anatase and rutile with the rutile fraction increasing with the temperature increase. The film morphology presents nanocrystalline conglomerates. The amorphous phase exists in the structure up to ∼700°C (Fig. 4b).

3. MB TiO_2 films demonstrate the crystallization process with a low nucleation rate and a large grain growth rate starting (and finishing after 1 to 2 h) at ~ 500°C and resulting in large grain (up to 5–10 μm in size) structure.
4. MB SnO_2 films show large-area monocrystalline growth over the NaCl substrate during their deposition. The crystallized phases are cassiterite and Sn-suboxides, often in mutually oriented multilayered structures (Fig. 4d).
5. The dominant structure of the SnO_2–TiO_2 films crystallized at 500–600°C is a mixture of rutile with cassiterite (in the case of RIS films, with a low SnO_2 content, Fig. 5a,b) or with Sn-suboxides (in the case of MB films, with a high SnO_2 concentration). In some large grains of the MB-films we have detected the lamellar growth originating possibly from the spinodal decomposition process (Fig. 5c). The crystallization of the MB-films often results in the precipitation of low-oxygen Sn-suboxides.

XRD and TEM analysis of the SnO_2–TiO_2 films both in the as-deposited state and after ex-situ and in-situ vacuum annealing show an obvious structural difference between films deposited by RIS or by MB-sputtering. In the last case (MB, high-temperature sputtering from initially molten state in vacuum), no stoichiometric SnO_2 (cassiterite) phase is observed and furthermore the titania phases were found also in the suboxide form. The films produced by RIS-processing in oxidation environment did not suffer of oxygen non-stoichiometry and show predominantly the cassiterite-anatase/rutile mixtures, at least in the as-deposited state and after low-temperature annealings in vacuum.

4. Summary

1. The crystallization processes of SnO_2–TiO_2 films deposited by means of RF-sputtering and molecular beam on SiO_2 and NaCl substrates have been investigated by means of electron microscopy, X-ray diffraction, Raman and IR spectroscopy to prove the model of the spinodal decomposition into the SnO_2–TiO_2 system at temperatures below 800°C.
2. The RIS films annealed in vacuum had decomposed into SnO_x and TiO_2 (anatase, rutile) mixtures at ~ 500 to 600°C. In the MB-films the decomposition is clearly expressed in the case of high SnO_2 ($=$ 50%) concentrations.
3. Further application of the molecular beam process (and, in general, the e-beam deposition in vacuum) of creating sensor structures needs the control of the oxygen stoichiometry by adding in situ atomic oxygen to the growing material or via the thin film oxidation after deposition.

Acknowledgements

The authors would like to thank Dr Mohammad Ghafari (Darmstadt TU), Dr Alex Berner (Technion), Ralf Nagel (Darmstadt TU) and Michael Schallehn (Darmstadt TU) for their help in the film deposition and in the measurements.

References

[1] S.R. Morrison, in: S.M. Sze (Ed.), Semiconductor Sensors, Wiley, New York, 1994, p. 383.
[2] G. Sberveglieri, Gas Sensors: Principles, Operation and Developments, Kluwer, The Netherlands, 1992, pp. 1–4.
[3] P.T. Mosely, B.C. Tofield, Solid State Gas Sensors, Adam Hilger, Bristol, 1987.
[4] F. Edelman, A. Rothshild, Y. Komem, V. Mikhelashvili, A. Chack, F. Cosandey, Electron Materials, A. Rothshild, F. Edelman, Y. Komem, F. Cosandey, Sensors and Actuators (in press).
[5] N.N. Padurow, Naturwissenschaften 43 (1956) 395.
[6] A.H. Schultz, V.S. Stubican, Phil. Mag. 18 (1968) 929.
[7] V.S. Stubican, A.H. Schultz, J. Am. Ceram. Soc. 51 (1968) 290.
[8] V.S. Stubican, A.H. Schultz, ibid 53 (1986) 211.
[9] D. Garcia, D. Speidel, ibid 55 (1972) 322.
[10] M. Park, T.E. Mitchell, A.H. Heuer, ibid 58 (1975) 43.
[11] M.F. Hennaut, P.H. Duvigneaud, E. Plumat, J. Physique 47 (1986) 1.
[12] Wan-Young Chung, Duk-Dong Lee, Byung-Ki Sohn, Thin Solid Films, 221 (1992) 304.
[13] K. Zakrzewska, M. Radecka, P. Pasierb, M. Bucko, E. Urbaniec, J. Janas, Acta Physica Polonica A91 (1997) 899.
[14] M. Radecka, K. Zakrzewska, M. Rekas, Sensors Actuators B47 (1998) 194.
[15] T. Hirata, K. Ishioka, M. Kitajima, H. Doi, Phys. Rev. B53 (1996) 8442.
[16] S. Arakawa, K. Mogi, K. Kikuta, T. Yogo, S. Hirano, J. Am. Ceram. Soc. 80 (1997) 2864.
[17] M. Radecka, K. Zakrzewska (unpublished).
[18] J.L. Murray (Ed.), Phase Diagram of Binary Titanium Alloys, ASM, International, OH, 1987.
[19] K.N. Yu, Y. Xiong, Y. Liu, C. Xiong, Phys. Rev. B55 (1997) 2666.
[20] L. Abello, B. Bochu, A. Gaskov, S. Koudryavtseva, G. Lucazeau, M. Roumyantseva, J. Solid State Chem. 135 (1998) 78.
[21] W. Ma, Z. Lu, M. Zhang, Appl. Phys. A66 (1998) 621.
[22] D. Bersani, P.P. Lottici, X.-Z. Ding, Appl. Phys. Lett. 72 (1998) 73.
[23] R.M. Cohen, D. Drobeck, A.V. Vicar, J. Am. Ceram. Soc. 171 (1988) 401.
[24] T. Hirata, K. Ishioka, M. Kitajima, H. Doi, Phys. Rev. B53 (1996) 8442.